Electronic Supplementary Material (ESI) for Materials Horizons.

Supporting Information

In situ Identification of Electrocatalytic Water Oxidation Behavior of Nickel-Based Metal-Organic Framework Nanoarray

Fanpeng Cheng,[1] Zhongjian Li,[1*] Lin Wang,[1] Bin Yang,[1,2] Jianguo Lu,[3] Lecheng Lei,[1,2] Tianyi Ma,[4*] Yang Hou[1,2,5*]

[1]Key Laboratory of Biomass Chemical Engineering of Ministry of Education, College of Chemical and Biological Engineering, Zhejiang University, Hangzhou 310027, China

[2]Institute of Zhejiang University - Quzhou, Quzhou 324000, China

[3]State Key Laboratory of Silicon Materials, School of Materials Science and Engineering, Zhejiang University, Hangzhou 310027, China

[4]Centre for Translational Atomaterials, Faculty of Science, Engineering and Technology, Swinburne University of Technology, Hawthorn, Victoria, 3122, Australia. E-mail: tianyima@swin.edu.au

[5]The Ningbo Research Institute, Zhejiang University, Ningbo 315100, China

Experimental section

Synthesis of OG. Graphite foil was firstly rinsed with acetone, ethanol, and deionized (DI) water under sonication for 20 min, respectively, and then dried in oven at 60 °C for 4 h. Next, an electrochemical exfoliation process was conducted by anodization of graphite foil in concentrated sulfuric acid with using Pt foil (10 mm × 10 mm) as counter electrode and graphite foil (30 mm × 30 mm) as working electrode under 5 V for 1 min.[1] The obtained electrode was rinsed with DI water several times and dried in oven at 60 °C.

Synthesis of NiBDC/OG. 119 mg of $NiCl_2 \cdot 6H_2O$ and 116 mg of 1,4-dicarboxybenzene acid (BDC) were dissolved in a mixed solvent of DI water, ethanol, and N,N-dimethylformamide (DMF) (18 mL, V:V:V = 1:1:16), and stirred for 20 min to form transparent solution. Then, as-obtained solution with a piece of OG foil (15 mm × 30 mm) was transferred into a Teflon-lined autoclave. Subsequently, the Teflon-lined autoclave was heated at 150 °C for 3 h in an oven, which was naturally cooled down to room temperature. The resulting electrode was washed with DMF, ethanol, and DI water, repeatedly, and then dried in oven at 60 °C. The loading amount of NiBDC on OG foil was ~0.64 mg cm^{-2}.

Synthesis of Ce-NiBDC/OG. 119 mg of $NiCl_2 \cdot 6H_2O$, 6.5 mg of $Ce(NO_3)_3 \cdot 6H_2O$, and 116 mg of 1,4-dicarboxybenzene acid (BDC) were dissolved in a mixed solvent of DI water, ethanol, and N,N-dimethylformamide (DMF) (18 mL, V:V:V = 1:1:16), and stirred for 20 min to form the transparent solution. Then, as-obtained solution with a piece of OG foil (15 mm × 30 mm) was transferred into a Teflon-lined autoclave. Subsequently, the Teflon-lined autoclave was heated at 150 °C for 3 h in an oven, which was naturally cooled down to room temperature. The resulting electrode was washed with DMF, ethanol, and DI water, repeatedly, and then dried in oven at 60 °C. The loading amount of Ce-NiBDC on OG foil was ~0.72 mg cm^{-2}.

The precursor ratio of Ce^{3+} to Ni^{2+} was regulated from 1% to 12% to synthesize the Ce-NiBDC with different molar ratios of Ce to Ni. Besides, we replaced the $Ce(NO_3)_3 \cdot 6H_2O$ with $MoCl_5$, WCl_6, $Cr(NO_3)_3 \cdot 9H_2O$, $CuCl_2 \cdot 2H_2O$, $CoCl_2 \cdot 6H_2O$, or $Fe(NO_3)_3 \cdot 9H_2O$ to synthesize the X-NiBDC/OG (X = Mo, W, Cr, Cu, Co, Fe).

The synthesis of Ce-NiBDC/OG-120 ^{o}C is similar to the synthesis of Ce-NiBDC/OG catalyst except the hydrothermal temperature was changed to 120 °C. The synthesis of Ce-NiBDC/OG-180 ^{o}C is similar to the synthesis of Ce-NiBDC/OG catalyst except the hydrothermal temperature was changed to 180 °C.

Synthesis of CeBDC/OG. 217 mg of $Ce(NO_3)_3 \cdot 6H_2O$ and 116 mg of 1,4-dicarboxybenzene acid (BDC) were dissolved in a mixed solvent of DI water, ethanol, and N,N-dimethylformamide (DMF) (18 mL, V:V:V = 1:1:16), and stirred for 20 min to form transparent solution. Then, as-obtained solution with a piece of OG foil (15 mm × 30 mm) was transferred into a Teflon-lined autoclave. Subsequently, the Teflon-lined autoclave was heated at 150 °C for 3 h in an oven, which was naturally cooled down to room temperature. The resulting electrode was washed with DMF, ethanol, and DI water, repeatedly, and then dried in oven at 60 °C. The loading amount of CeBDC on OG foil was ~0.54 mg cm^{-2}.

Characterizations: The morphologies of samples were examined by FESEM (Hitachi SU-8010), TEM (HT7700), and HRTEM (JEOL JEM-2001F). The crystal structures of catalysts were measured by XRD (Empyrean 200895) using Cu Kα radiation. The chemical environments of samples were measured by XPS (Escalab 250Xi) with Al Kα radiation. Raman spectra of samples were measured with a LabRAM HR Evolution. The N_2 adsorption-desorption curves of samples were tested by BET (ASIC-2). The metal content in catalysts was analyzed by ICP-MS (Vista Axial). XAS measurements of Ce-NiBDC/OG and the control samples were tested in Beijing Synchrotron Radiation Facility and Shanghai Synchrotron Radiation Facility.

Electrochemical measurements: All electrochemical measurements were carried out by an electrochemical analyzer (CHI 760E) in a typical three-electrode configuration. A saturated Ag/AgCl electrode and a graphite rod were used as reference electrode and counter electrode, respectively. The potential was converted to reversible hydrogen electrode (RHE) via a Nernst equation ($E_{RHE} = E_{Ag/Ag/Cl} + 0.059 \times pH + 0.197$). To evaluate the OER activities of catalysts, the scan rate of linear sweep voltammetry (LSV) was set to 1.0 mV s^{-1} with the potentials between 0 V and 0.8 V vs. Ag/AgCl in 1.0 M KOH. Electrochemical impedance spectroscopy (EIS) was

measured at 0.5 V vs. Ag/AgCl with a frequency range from 10^5 Hz to 0.01 Hz. All polarization curves were calibrated with iR correction unless noted. Cyclic voltammetry cycles (CVs) at 0.8 V - 1.0 V vs. RHE with the scan rates from 20 - 100 mV s^{-1} was applied to analyze electrochemically active surface area (ECSA).

Calculation method: The present DFT calculations based on the first principle are performed by Vienna Ab initio Simulation Package (VASP) with the projector augmented wave (PAW) method.[2, 3] The exchange-functional is treated using the generalized gradient approximation (GGA) of Perdew-Burke-Ernzerhof (PBE) functional.[4] The energy cutoff for the plane wave basis expansion is set to 450 eV and the force on each atom less than 0.03 eV $Å^{-1}$ is set for the convergence criterion of geometry relaxation. The Brillouin zone integration is performed using 3×3×1 k-point sampling through all the computational processes of OER. The supercell is constructed by a five-layer 3×1 NiOOH (011) slab and a 15 Å vacuum, in order to avoid the interaction between periodic structures. The self-consistent calculations apply a convergence energy threshold of 10^{-4} eV. To describe vdW interaction, empirical Grimme's D3 correction is adopted. The Free energies of the OER steps are calculated using equation:[5]

$\Delta G = \Delta E_{DFT} + \Delta E_{ZPE} - T\Delta S$

where ΔE_{DFT} is the DFT energy difference, and the ΔE_{ZPE} and $T\Delta S$ terms are obtained based on vibration analysis. The corrections of zero point energy and entropy of different species are shown in Table S4.

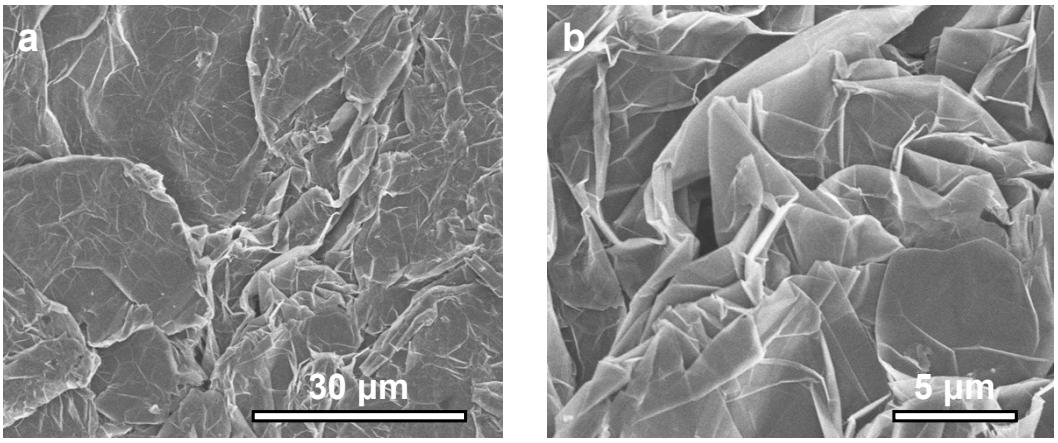

Figure S1. (a-b) FESEM images of 3D OG foil.

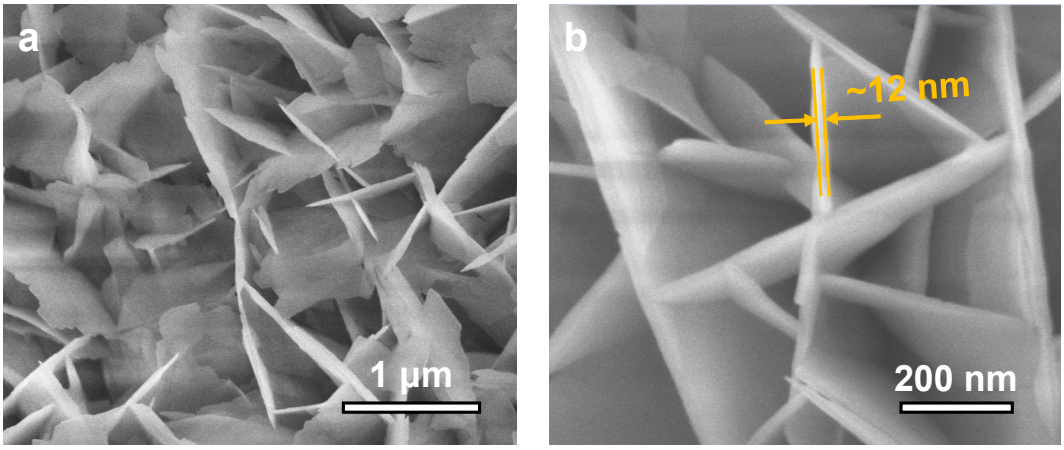

Figure S2. (a-b) FESEM images of Ce-NiBDC/OG.

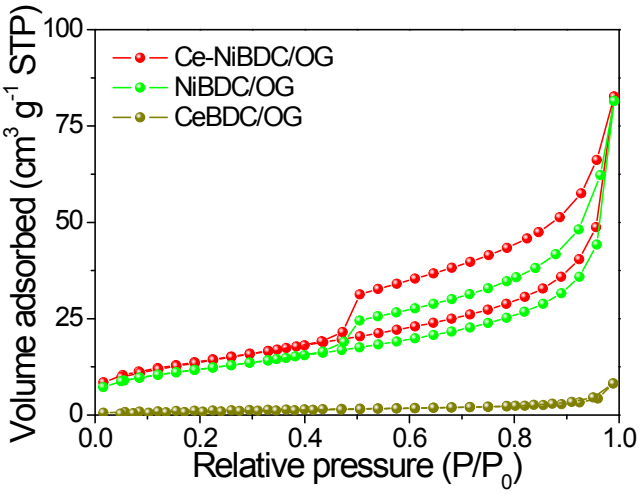

Figure S3. N_2 adsorption-desorption isotherm curves of Ce-NiBDC/OG, NiBDC/OG, and CeBDC/OG.

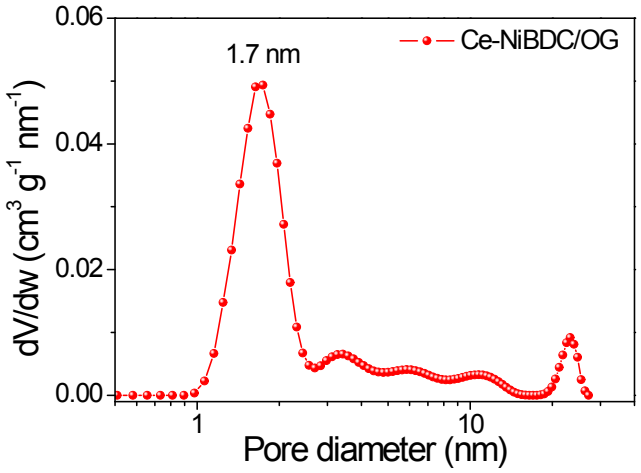

Figure S4. Pore size distribution of Ce-NiBDC/OG.

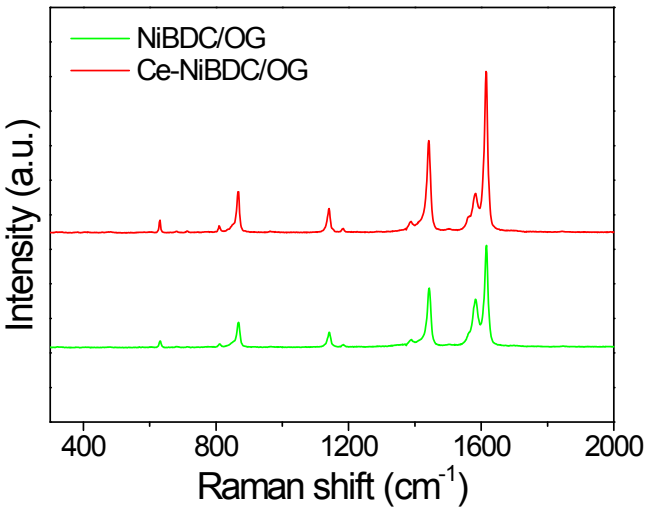

Figure S5. Raman spectra of Ce-NiBDC/OG and NiBDC/OG.

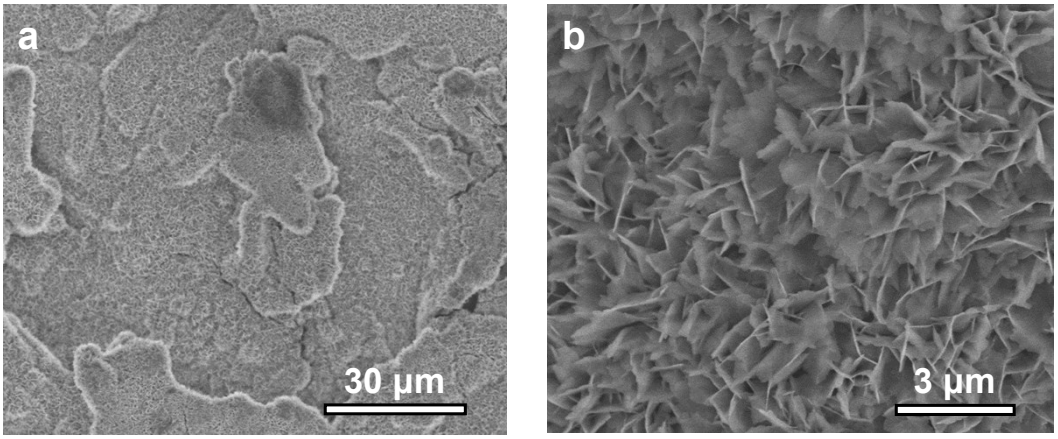

Figure S6. (a-b) FESEM images of NiBDC/OG.

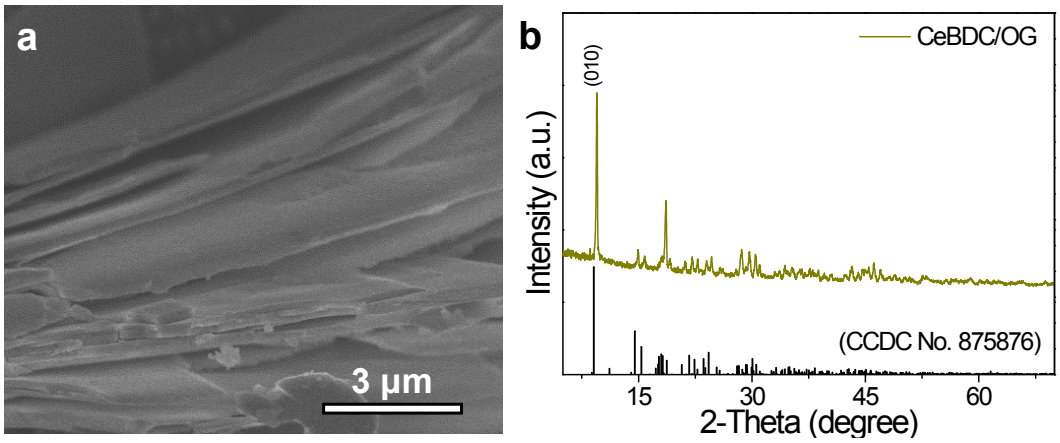

Figure S7. (a-b) FESEM image and XRD pattern of CeBDC/OG.

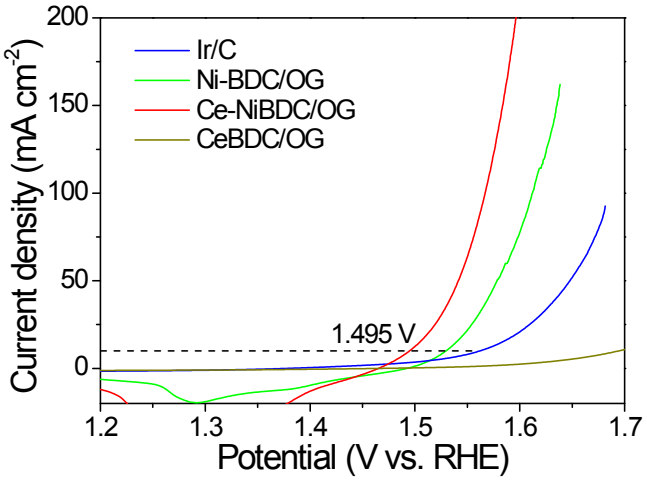

Figure S8. Reverse polarization curves of Ir/C, NiBDC/OG, Ce-NiBDC/OG, and CeBDC/OG.

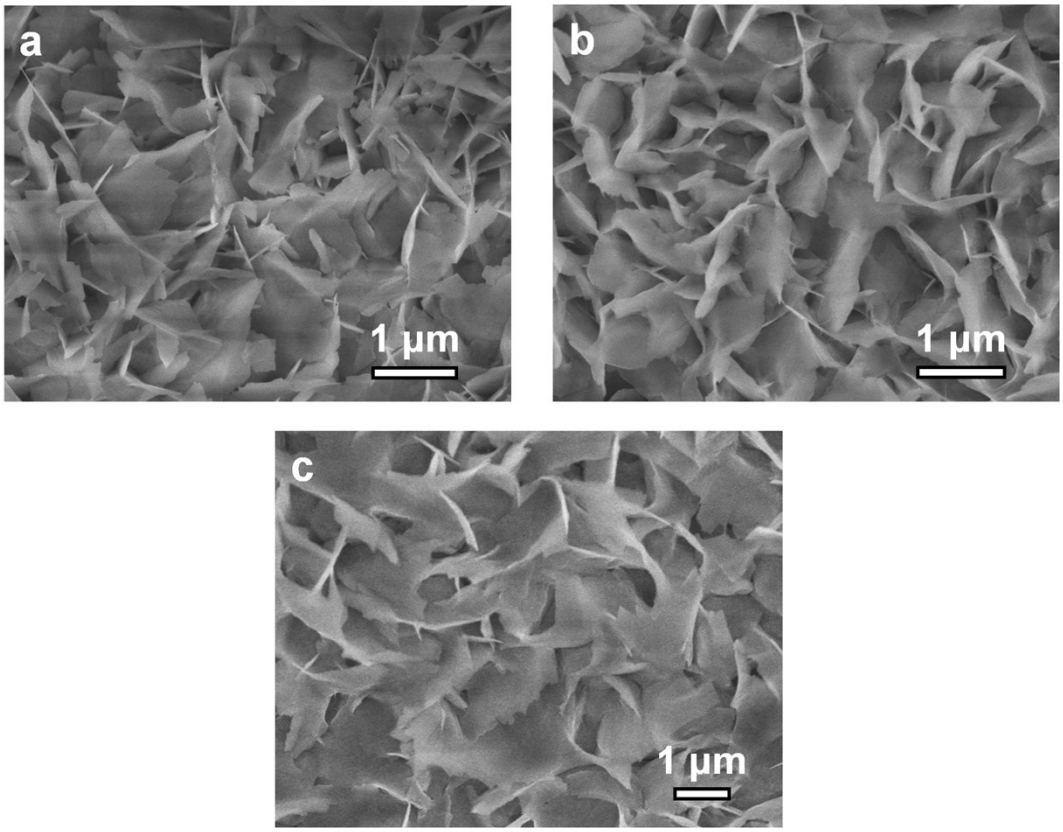

Figure S9. FESEM images of (a) 0.66 wt.% Ce doping, (b) 3.33 wt.% Ce doping, and (c) 5.12 wt.% Ce doping.

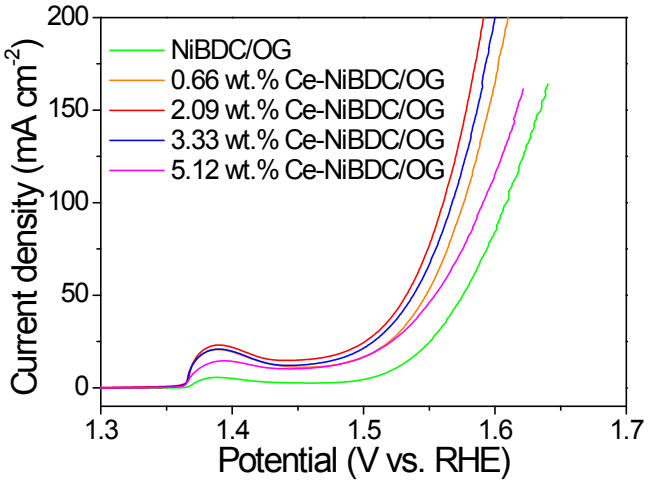

Figure S10. Polarization curves of NiBDC/OG with different loading amounts of Ce species.

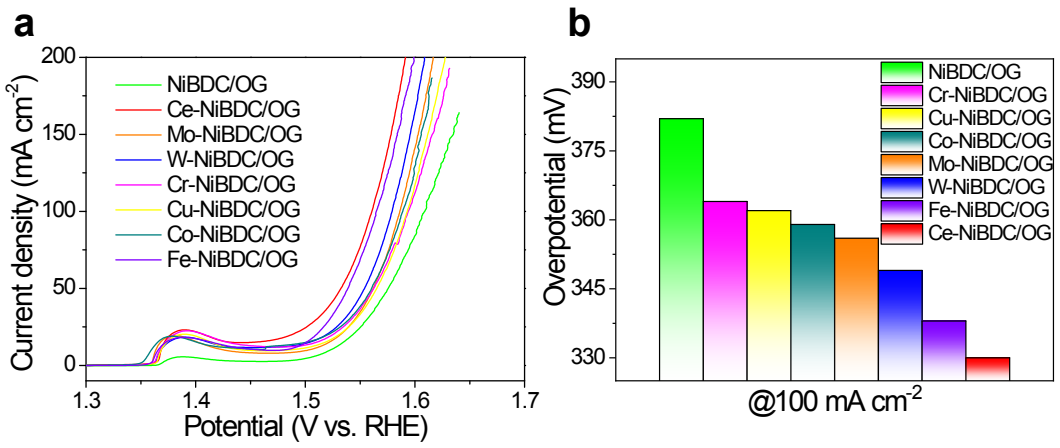

Figure S11. (a) Polarization curves of NiBDC/OG with different metal doping. (b) Corresponding overpotentials at 100 mA cm^{-2}.

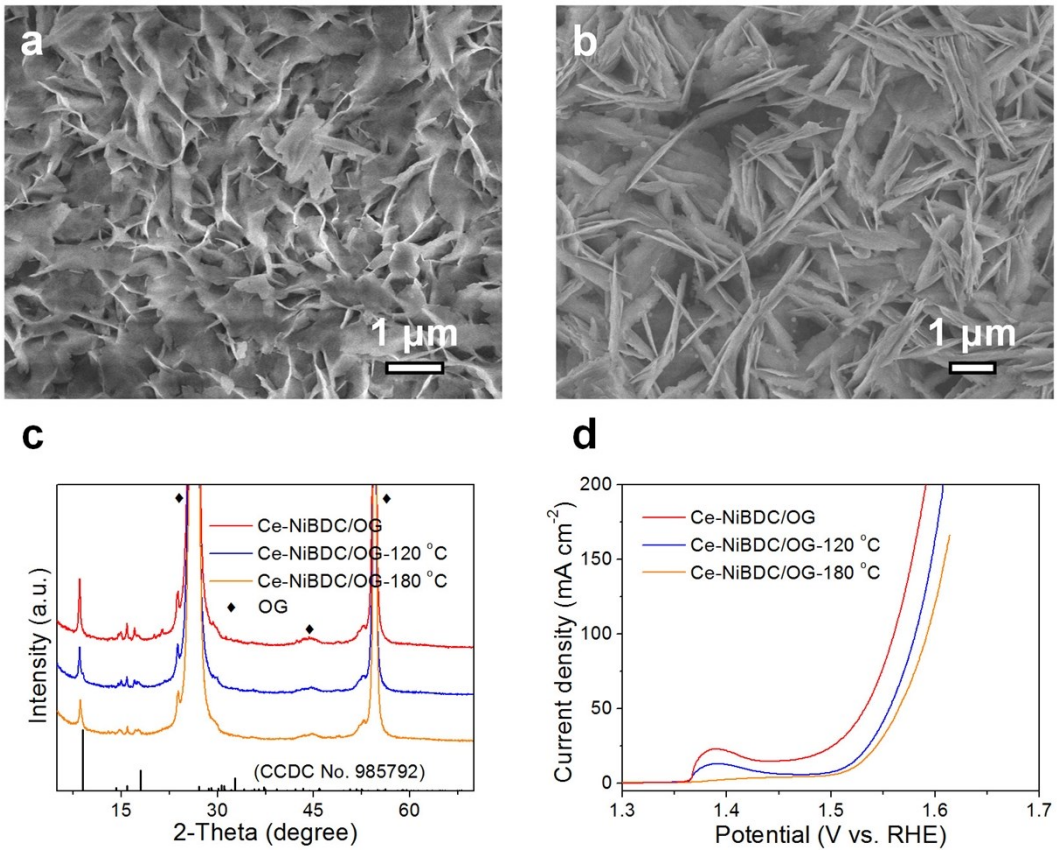

Figure S12. FESEM images of Ce-NiBDC/OG synthesized under different temperatures for (a) Ce-NiBDC/OG-120 °C and (b) Ce-NiBDC/OG-180 °C. (c) XRD patterns and (d) polarization curves of Ce-NiBDC/OG, Ce-NiBDC/OG-120 °C, and Ce-NiBDC/OG-180 °C.

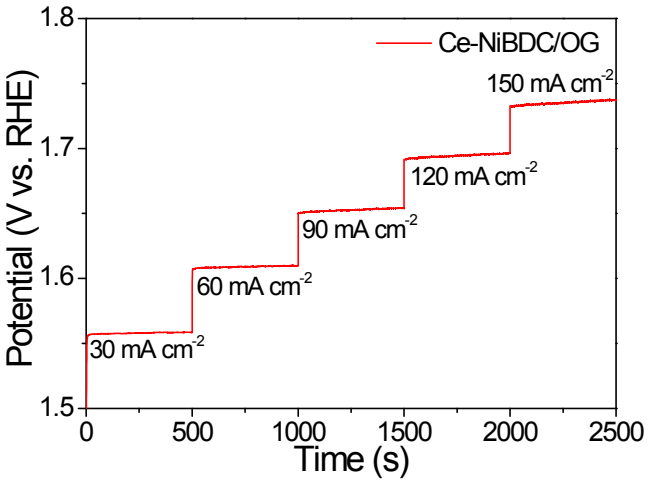

Figure S13. Multi-step chronopotentiometric curve of Ce-NiBDC/OG.

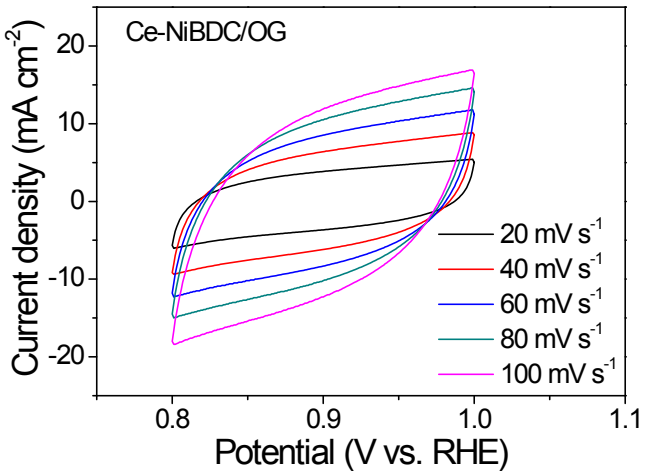

Figure S14. CV curves of Ce-NiBDC/OG at different scan rates in 1.0 M KOH solution.

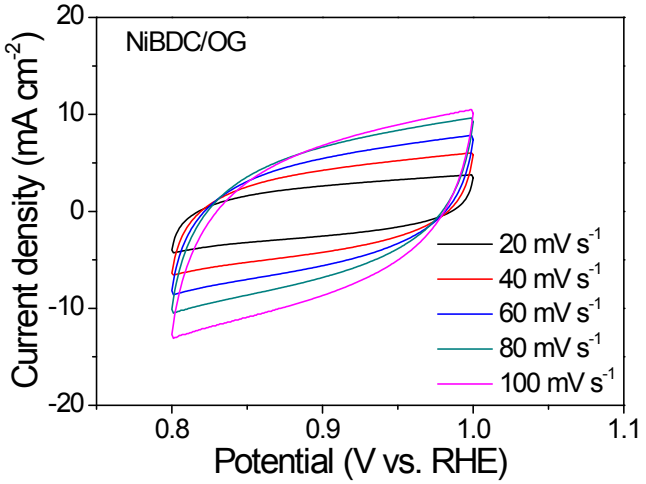

Figure S15. CV curves of NiBDC/OG at different scan rates in 1.0 M KOH solution.

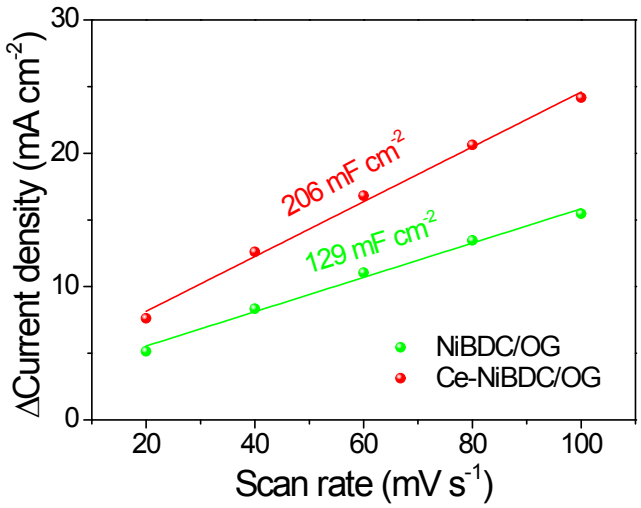

Figure S16. ECSAs of NiBDC/OG and Ce-NiBDC/OG.

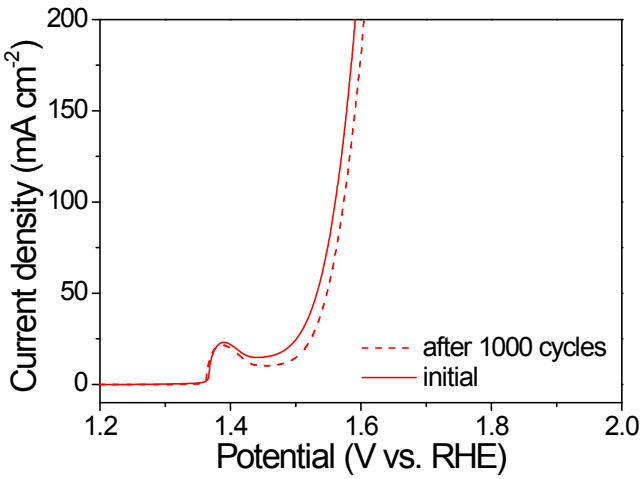

Figure S17. Polarization curves of Ce-NiBDC/OG before and after 1000 CV cycles.

The polarization curve of Ce-NiBDC/OG demonstrates an inconspicuous loss even after 1000 CV cycles, implying its high stability and durability for OER in alkaline media.

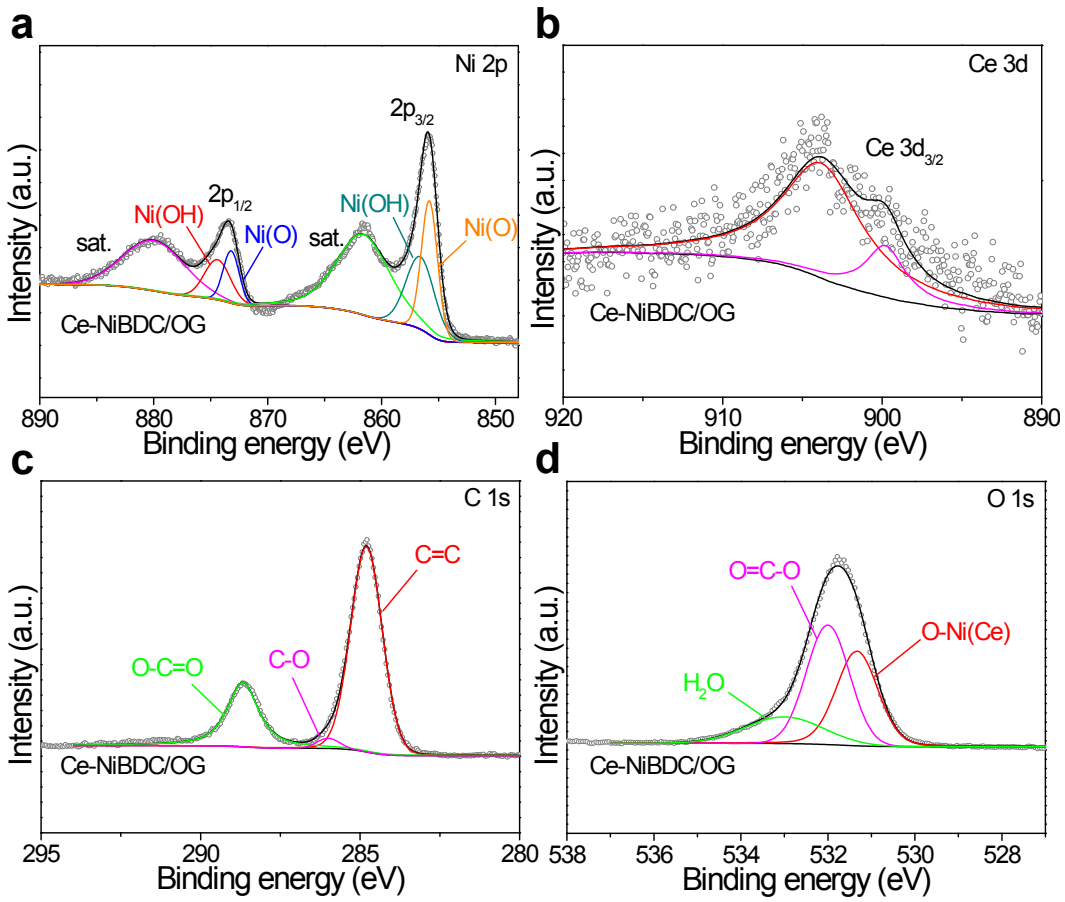

Figure S18. High-resolution XPS spectra for (a) Ni 2p, (b) Ce 3d, (c) C 1s, and (d) O 1s of Ce-NiBDC/OG.

The binding energies at around 855.8 eV and 873.3 eV could be assigned to the Ni-O bonds between Ni atoms and BDC molecules. The binding energies at around 856.9 eV and 874.5 eV could be assigned to the Ni-OH bonds between Ni atoms and hydroxyl groups with two shakeup satellite peaks at 880.0 and 861.6 eV.[6]

The high-resolution XPS spectrum of C 1s was deconvoluted into three surface components, corresponding to the benzene rings of BDC linkers at 284.8 eV, O-C=O bonds at 288.7 eV, and C-O bonds at 286.0 eV. The high-resolution XPS spectrum of O 1s could be fitted by three peaks centered at 531.3, 532, and 533.0 eV, attributed to the O atoms on the Ni(Ce)-O bonds, the carboxylate groups in BDC linkers, and absorbed water, respectively.[7]

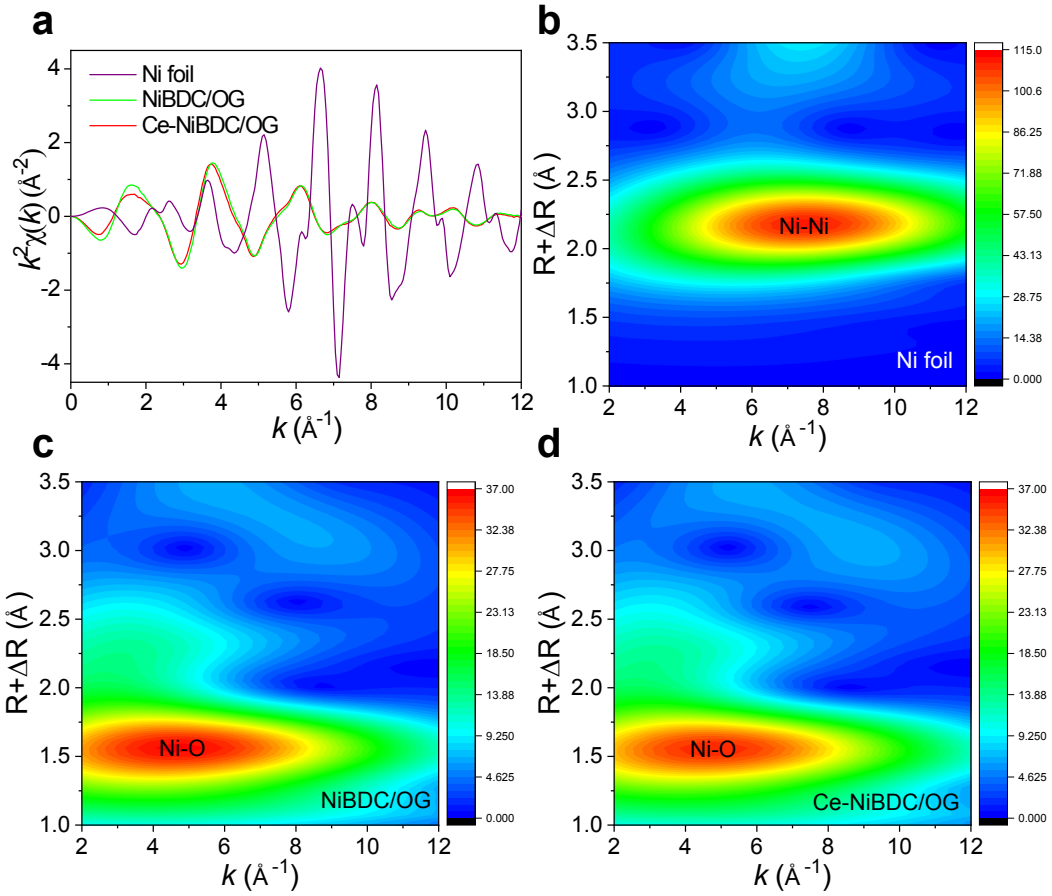

Figure S19. (a) The k-space of Ni K-edge EXAFS spectra and (b-d) wavelet transforms for Ni foil, NiBDC/OG, and Ce-NiBDC/OG.

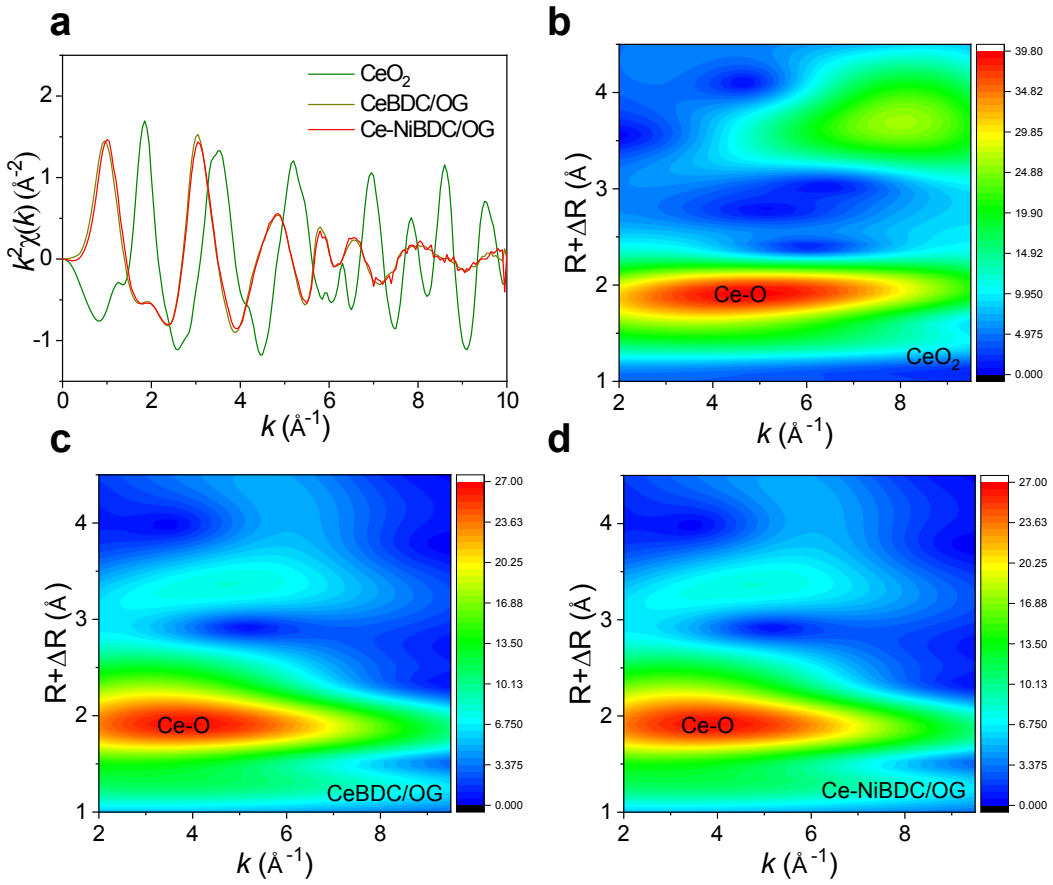

Figure S20. (a) The k-space of Ce L-edge EXAFS spectra and (b-d) wavelet transforms for CeO_2, CeBDC/OG, and Ce-NiBDC/OG.

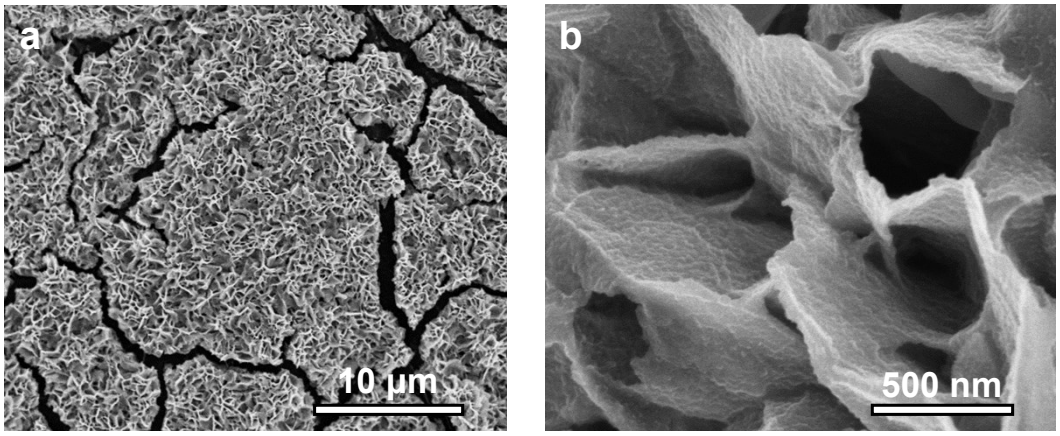

Figure S21. (a-b) FESEM images of Ce-NiBDC/OG after OER electrocatalysis.

The inherited nanosheets array morphology remains with the appearance of several coarse wrinkles.

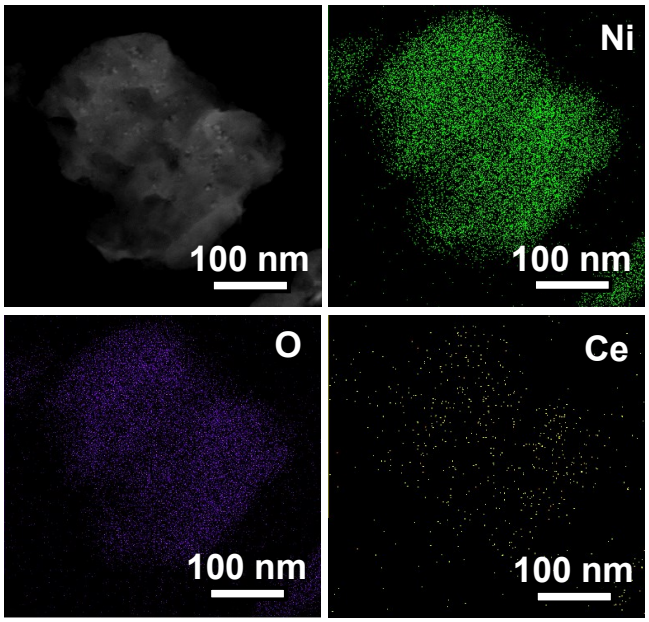

Figure S22. HAADF-STEM and element mapping images of Ce-NiBDC/OG after OER electrocatalysis.

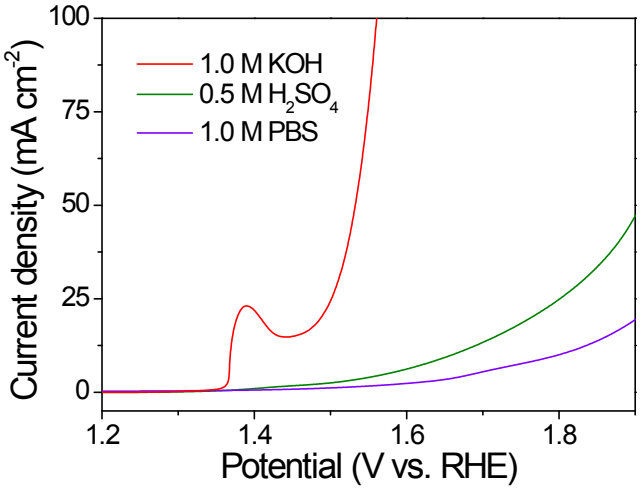

Figure S23. Polarization curves of Ce-NiBDC/OG in 1.0 M KOH, 0.5 M H_2SO_4, and 1.0 M PBS (pH = 7.0).

In both acid and neutral media, the Ce-NiBDC/OG did not show high OER activity as in alkaline media, possibly due to the incapable of phase transformation into the high-active Ce-NiOOH species that is also unstable in acid media.

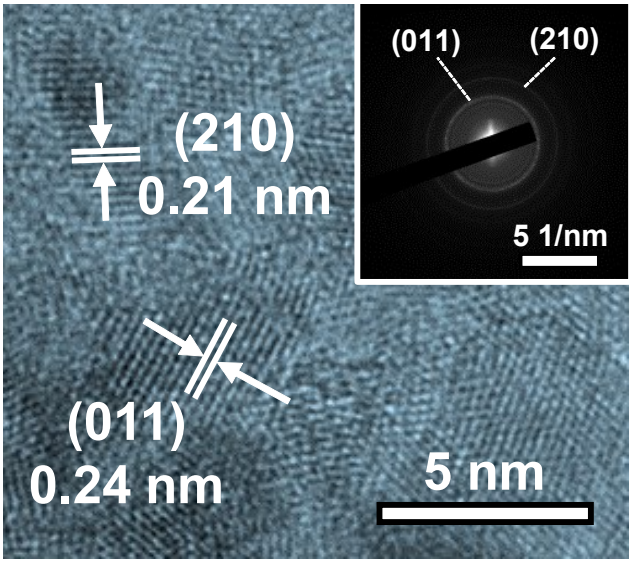

Figure S24. HRTEM image of Ce-NiBDC/OG after OER electrocatalysis. Inset: corresponding SAED pattern.

The post- HRTEM image of Ce-NiBDC/OG still presents the well-defined lattice fringe spacings, demonstrating good crystallinity of in-situ generated Ce-NiOOH derived from Ce-NiBDC/OG.

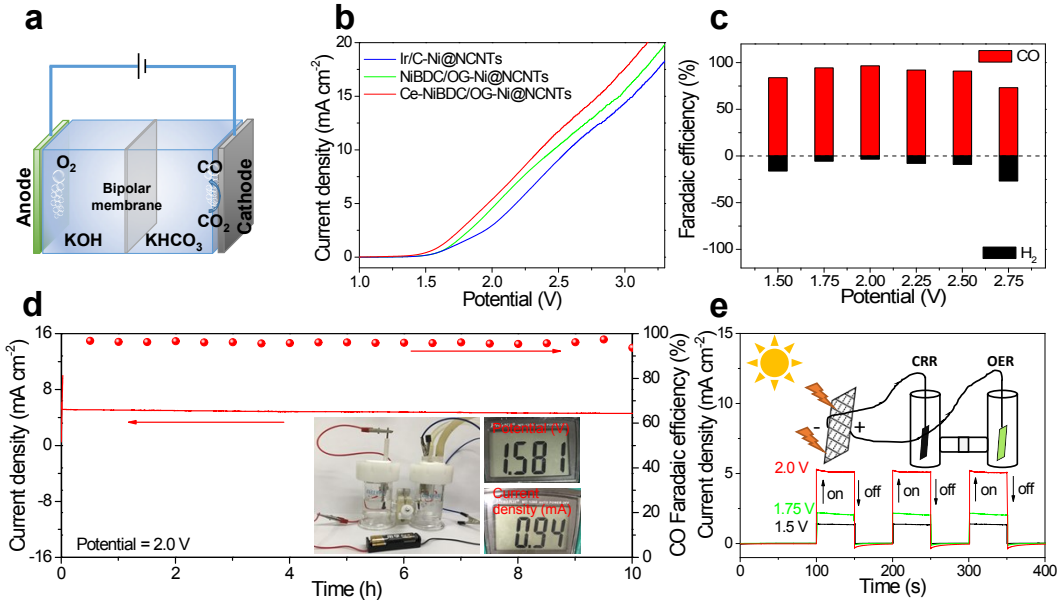

Figure S25. (a) Schematic illustration of alkaline-neutral OER-CRR cell. (b) Polarization curves of Ir/C-Ni@NCNTs, NiBDC/OG-Ni@NCNTs, and Ce-NiBDC/OG-Ni@NCNTs in two-electrode system. (c) CO F.E. of Ce-NiBDC/OG-Ni@NCNTs. (d) CO F.E. and chronoamperometric curve under 2.0 V. (e) Photocurrent densities of OER-CRR device at different applied potentials powered by solar panel under simulated sunlight (AM 1.5G, 100mW cm^{-2}).

Encouraged by highly efficient OER activity of Ce-NiBDC/OG, we further established a fuel cell that combined Ni@NCNTs as cathode for CO_2 electroreduction and Ce-NiBDC/OG as anode for OER. For OER reaction, compared with that of Ir/C (2.58 V) and NiBDC/OG (2.46 V), a low potential of 2.36 V was required to reach 10 mA cm^{-2} for Ce-NiBDC/OG. The Ni@NCNTs can achieve high selectivity for CO production with the maximum Faradaic efficiency (F.E.) of 96.55% at 2.0 V, which can be started by one battery. Additionally, the current density under 2.0 V showed an insignificant loss over 10 h along with immobile CO F.E., suggesting its high stability. The cell displayed a rapid and retrievable transient photocurrent response with ON/OFF illumination circulation under simulated sunlight irradiation at different potentials, implying robust charge transport property.

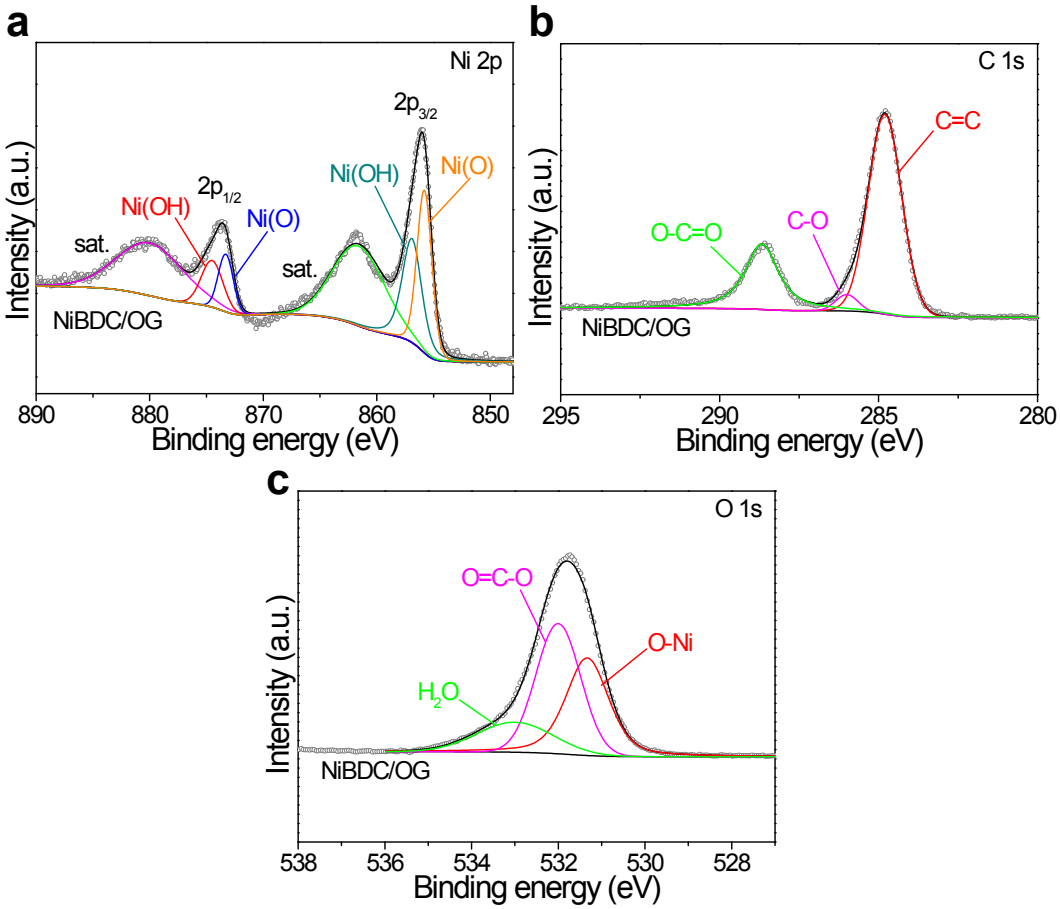

Figure S26. High-resolution XPS spectra for (a) Ni 2p, (b) C 1s, and (c) O 1s of NiBDC/OG.

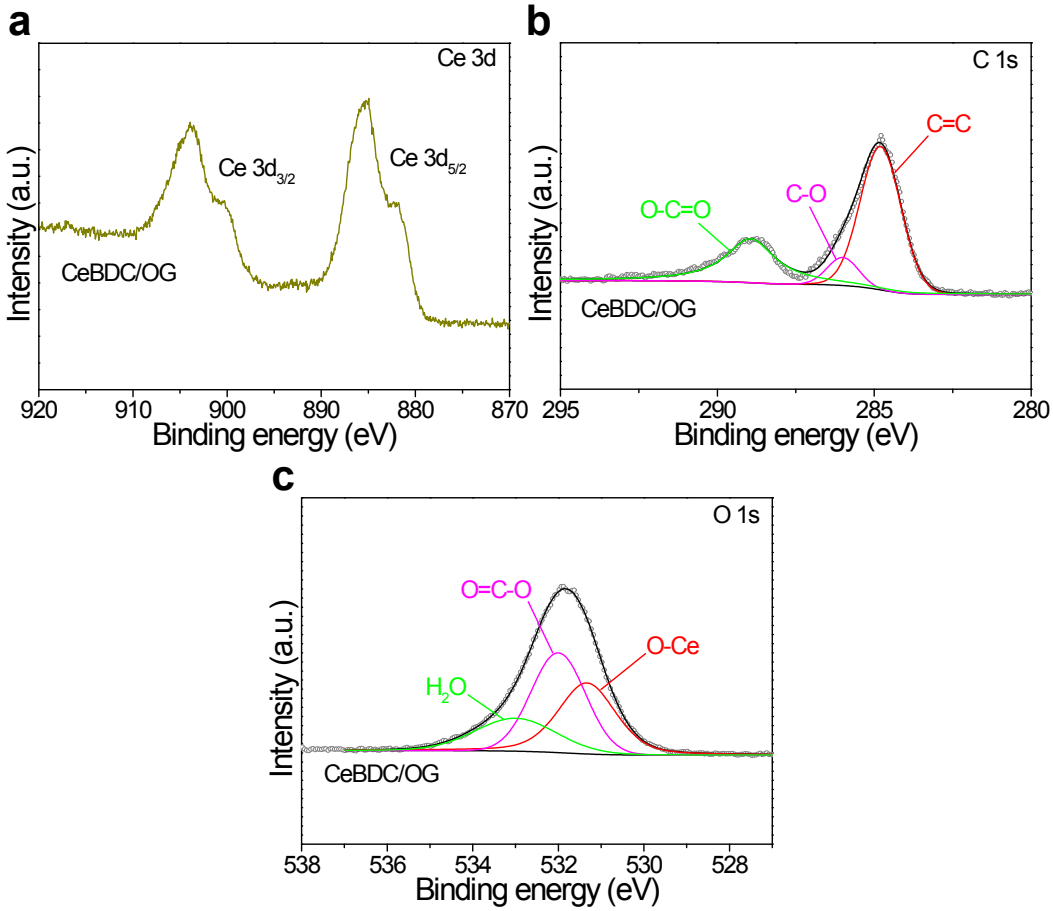

Figure S27. High-resolution XPS spectra for (a) Ce 3d, (b) C 1s, and (c) O 1s of CeBDC/OG.

Figure S28. Static-water-droplet contact angles of NiBDC/OG.

Table S1. The EIS results of Ce-NiBDC/OG with other control electrodes in 1.0 M KOH solution in this work.

Sample electrode	R_s/Ω	R_{ct}/Ω
CeBDC/OG	1.33	54.1
Ir/C	1.34	15.7
NiBDC/OG	1.22	5.16
Ce-NiBDC/OG	0.93	1.73

Table S2. Comparison of electrocatalytic OER performances of Ce-NiBDC/OG with other reported MOF-based OER catalysts in alkaline media.

Catalyst	electrolyte	Overpotential @10 mA cm^{-2}	Tafel slope ($mV\ dec^{-1}$)	Ref.
Ni-UMOFNs	1.0 M KOH	321	65	[8]
Ni-MOF@Fe-MOF	1.0 M KOH	265	82	[7]
$A_{2.7}B$-MOF-$FeCo_{1.6}$	1.0 M KOH	288	39	[9]
$(Ni_2Co_1)_{0.925}Fe_{0.075}$-MOF-NF	1.0 M KOH	257	41.3	[10]
Co-BDC/$Ti_3C_2T_x$	1.0 M KOH	410	48.2	[11]
MAF-X27-OH	pH=14	320	66	[12]
NNU-23	0.1 M KOH	365	77.2	[13]
Co-WOC-1	0.1 M KOH	390	128	[14]
CUMSs-ZIF-67	1.0 M KOH	320	53.7	[15]
Ce-NiBDC/OG	**1.0 M KOH**	**265**	**46**	**This work**

Table S3. Fitting parameters of Ni K-edge and Ce L-edge EXAFS curves for Ce-NiBDC/OG first shell.

Path	Coordination number (CN)	Bond distance (R (Å))	ΔE_0 (eV)	σ^2 (10^{-3} Å^2)	R-factor
Ni-O	5.8 (6) ± 0.3	2.03 ± 0.02	-2.0	5.6 ± 0.6	0.007
Ce-O	6.1 (6) ± 0.4	2.38 ± 0.03	-3.8	7.4 ± 0.8	0.009

Table S4. The correction values of zero point energy and entropy of the adsorbed species.

	ZPE (eV)	TS (eV)
*OH	0.365	0.098
*O	0.066	0.049
*OOH	0.458	0.156

References

1 C. Lei, Q. Zheng, F. Cheng, Y. Hou, B. Yang, Z. Li, Z. Wen, L. Lei, G. Chai and X. Feng, *Adv. Funct. Mater.*, 2020, **30**, 2003000.

2 G. Kresse and J. Furthmüller, *Comput. Mater. Sci.*, 1996, **6**, 15-50.

3 P. E. Blöchl, *Phys. Rev. B*, 1994, **50**, 17953-17979.

4 J. P. Perdew, J. A. Chevary, S. H. Vosko, K. A. Jackson, M. R. Pederson, D. J. Singh and C. Fiolhais, *Phys. Rev. B*, 1992, **46**, 6671-6687.

5 J. Rossmeisl, A. Logadottir and J. K. Nørskov, *Chem. Phys.*, 2005, **319**, 178-184.

6 W. Li, F. Li, H. Yang, X. Wu, P. Zhang, Y. Shan and L. Sun, *Nat. Commun.*, 2019, **10**, 5074.

7 K. Rui, G. Zhao, Y. Chen, Y. Lin, Q. Zhou, J. Chen, J. Zhu, W. Sun, W. Huang and S. X. Dou, *Adv. Funct. Mater.*, 2018, **28**, 1801554.

8 S. Zhao, Y. Wang, J. Dong, C.-T. He, H. Yin, P. An, K. Zhao, X. Zhang, C. Gao, L. Zhang, J. Lv, J. Wang, J. Zhang, A. M. Khattak, N. A. Khan, Z. Wei, J. Zhang, S. Liu, H. Zhao and Z. Tang, *Nat. Energy*, 2016, **1**, 16184.

9 Z. Xue, Y. Li, Y. Zhang, W. Geng, B. Jia, J. Tang, S. Bao, H.-P. Wang, Y. Fan, Z.-w. Wei, Z. Zhang, Z. Ke, G. Li and C.-Y. Su, *Adv. Energy Mater.*, 2018, **8**, 1801564.

10 Q. Qian, Y. Li, Y. Liu, L. Yu and G. Zhang, *Adv. Mater.*, 2019, **31**, e1901139.

11 L. Zhao, B. Dong, S. Li, L. Zhou, L. Lai, Z. Wang, S. Zhao, M. Han, K. Gao, M. Lu, X. Xie, B. Chen, Z. Liu, X. Wang, H. Zhang, H. Li, J. Liu, H. Zhang, X. Huang and W. Huang, *ACS Nano*, 2017, **11**, 5800-5807.

12 X.-F. Lu, P.-Q. Liao, J.-W. Wang, J.-X. Wu, X.-W. Chen, C.-T. He, J.-P. Zhang, G.-R. Li and X.-M. Chen, *J. Am. Chem. Soc.*, 2016, **138**, 8336-8339.

13 X.-L. Wang, L.-Z. Dong, M. Qiao, Y.-J. Tang, J. Liu, Y. Li, S.-L. Li, J.-X. Su and Y.-Q. Lan, *Angew. Chem. Int. Ed.*, 2018, **57**, 9660-9664.

14 P. Manna, J. Debgupta, S. Bose and S. K. Das, *Angew. Chem. Int. Ed.*, 2016, **55**, 2425-2430.

15 L. Tao, C.-Y. Lin, S. Dou, S. Feng, D. Chen, D. Liu, J. Huo, Z. Xia and S.

Wang, *Nano Energy*, 2017, **41**, 417-425.